Original Research

Surface sulfonation and nitrification enhance the biological activity and osteogenesis of polyetheretherketone by forming an irregular nano-porous monolayer

Yanhua Li[1,2] · Jing Wang[3] · Dong He[1,2] · GuoxiongZhu[3] · Gaoyi Wu[3] · Lei Chen[1,2]

Abstract

Polyether-ether-ketone (PEEK) is becoming a popular component of clinical spinal and orthopedic applications, but its practical use suffers from several limitations. In this study, irregular nano-porous monolayer with differently functional groups was formed on the surface of PEEK through sulfonation and nitrification. The surface characteristics were detected by field-emission scanning electron microscopy, atomic force microscopy, energy-dispersive X-ray spectrometry, water contact angle measurements and Fourier transform infrared spectroscopy. In vitro cellular behaviors were evaluated by cell adhesion, morphological changes, proliferation, alkalinity, phosphatase activity, real-time RT-PCR and western blot analyses. In vivo osseointegration was examined through micro-CT and histological assessments. Our results reveal that the irregular nano-porous of PEEK affect the biological properties. High-temperature hydrothermal NP treatment induced early osteogenic differentiation and early osteogenesis. Modification by sulfonation and nitrification can broaden the use of PEEK in orthopedic and dental applications. This study provides a theoretical basis for the wider clinical application of PEEK.

These authors contributed equally: Yanhua Li, Jing Wang, Dong He

✉ Lei Chen
   sddxchenlei@163.com

1   Shandong Provincial Key Laboratory of Oral Tissue Regeneration, School of Stomatology, Shandong University, Wenhua Xi Road No. 44-1, Jinan 250012 Shandong, PR China

2   Department of Orthodontics, School of Stomatology, Shandong University, Jinan, Shandong, PR China

3   Department of Stomatology, PLA 960th hospital, Jinan 250031 Shandong, PR China

Graphical Abstract

a To obtain a uniform porous structure, PEEK samples were treated by concentrated sulfuric acid and fuming nitric acid (82–80%) with magnetic stirring sequentially. **b** Effects of nanopores on biological behavior of bMSCS.
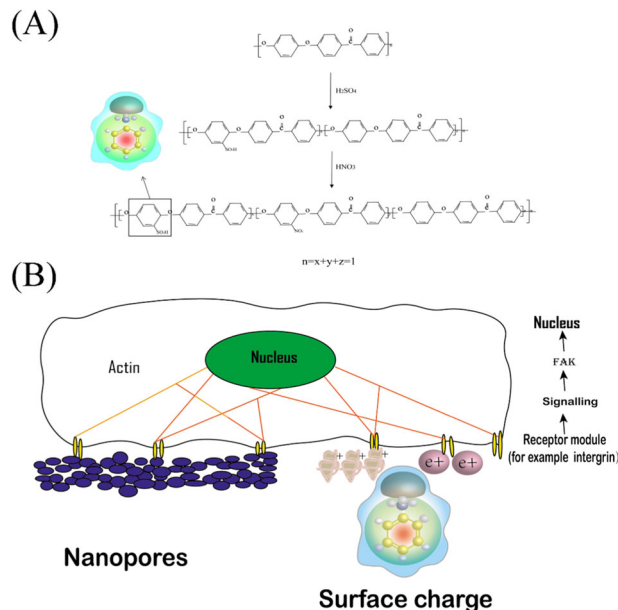
1 Introduction

Promoting rapid healing and safely integrating with bone are standards for selecting implant materials for dental and orthopedic implants. Traditional metal biomaterials, such as titanium and its alloys, have excellent corrosion resistance, high mechanical strength, and good cytocompatibility. However, metal materials release potentially harmful ions and have large elastic moduli that are ~6–20 times greater than that of bone, which results in bone resorption [1]. Nevertheless, better alternative materials are currently not available in clinic. PEEK has attracted extensive attention as a substitute for traditional metallic implant applications [2, 3]. PEEK has excellent mechanical properties, including elasticity, stiffness, tensile strength and resistance to distortion, abrasion and fatigue, which are within the proper ranges to coexist with human bone [4]. PEEK also has good chemical resistance compared with metal implants, which can prevent the degradation caused by corrosion. Additionally, the elastic modulus of PEEK (4–5 Gpa) is similar to that of cortical bone (18 Gpa) [5]. Therefore, PEEK is commonly used in spine fusion and artificial joint replacement and has become an attractive material in the field of stomatology.

Although PEEK has excellent mechanical properties, chemical resistance and has an elastic modulus which is similar with that of normal human bone, it is bioinert and limited local bone attachment. Nanostructures can promote

stem cell differentiation. Previous studies [6, 7] have demonstrated that the pore features (size and depth) on Ti surfaces have a greater effect on cell growth and osteogenic capacity. A three-dimensional (3D) porous network was previously generated on PEEK samples by sulfonation (SP) and enhanced the hydrophobicity and bioactivity of the surface [8]. To obtain surface porosity on PEEK, the melt extrusion technique has been used to form a microporous structure. They demonstrated that microporous PEEK could provide improved osseointegration while maintaining its integrity as a load-bearing structure [9, 10]. Some studies have found that nanostructures can promote the differentiation of stem cells. Nevertheless, irregular smaller-pore structures are relatively less frequently formed on the surface of PEEK due to the inherent chemical resistance of PEEK especially in the absence of the introduction of other bioactive materials such as Ti and HA.

In the study, sulfonation and nitrification treatment produces irregular monolayer nano-pores with diameters between 200 nm and 300 nm on the PEEK samples. This technique has the advantage of simple operation characteristic, thus boding well for biomedical implants. The advantages of sulfonation and nitrification treatment also contains the introduction of new functional groups, such as SO_3H and NO_2 groups. In the present study, we preliminarily explored the structure of irregular nano-porous and systematically evaluated the biological function of the nano-porous monolayer of PEEK samples in vivo and in vitro.

2 Materials and methods

2.1 Sample preparation and experimental design

Biomedical grade PEEK (Invibio, UK) was machined into samples with different dimensions. Square samples with dimensions of 10 mm × 10 mm × 1 mm was prepared for surface characterization and in vitro studies in 24-well tissue culture plates, while square samples with dimensions of 15 mm × 15 mm × 1 mm were used for real-time PCR and western blot assessments. Rod-shaped samples (diameter: 2 mm, length: 5 mm) were used in the in vivo studies. All the samples were polished and ultrasonically cleaned in acetone, ethanol and deionized water. To obtain a uniform porous structure, magnetic stirring was utilized throughout most of the process. According to different treatments, PEEK samples were divided into 5 groups. (1) PEEK group: no operation; (2) NP group: PEEK was treated with concentrated sulfuric acid (95–98 wt%, Aldrich Chemical Corp) and fuming nitric acid (82–80%) with magnetic stirring for 1 min at 16 °C sequentially. And immersed in deionized water at room temperature (25 °C) for 4 h. (3) 100NP group: PEEK was treated with concentrated sulfuric acid (95–98 wt%, Aldrich Chemical Corp) and fuming nitric acid (82–80%) with magnetic stirring for 1 min at 16 °C sequentially. And immersed in deionized water at 100 °C for 4 h. (4) SP group: PEEK was sulfonated in concentrated sulfuric acid (95–98 wt%, Aldrich Chemical Corp) and kept at room temperature for 1 min and immersed in deionized water at room temperature (25 °C) for 4 h. (5) 100SP group: PEEK was sulfonated in concentrated sulfuric acid (95–98 wt%, Aldrich Chemical Corp) and kept at room temperature for 1 min and immersed in deionized water at 100 °C for 4 h.

2.2 Surface characterization

The surface topography of the prepared samples was examined by field-emission scanning electron microscopy (FE-SEM; JEOL JSM-4800, Hitachi Corporation, Japan). ImageJ software was used to measure the pore size of the samples. Atomic force microscopy (5500, Agilent, Germany) was used to record the 3D morphologies of the sample surfaces. The elemental compositions and distributions of the specimens were examined by energy-dispersive X-ray spectrometry (EDS; INCA Energy, UK). The Fourier transform infrared (FTIR) spectra were recorded using aVertex70 system manufactured by Bruker. The water contact angle was used to determine the surface hydrophobicity at ambient humidity and temperature (FM40, Kruss, Germany).

2.3 In vitro studies

2.3.1 Cell culture

The rat bone mesenchymal stem cells (bMSCs) used in this study were routinely cultured.

2.3.2 Cell adhesion

The adhesion ability of cells was evaluated by observing the number of cells on the surface of the material. The bMSCs were seeded on the samples in a 24-well plate at a density of 2×10^4 cells per well and cultured for 4 h. The nuclei were stained with 40,60-diamidino-2-phenylindole (DAPI, Solarbio) for 8 min.

2.3.3 Cell morphology

2.3.3.1 FE-SEM The initial cell adhesion morphology was observed by SEM. The bMSCs were seeded on specimens in a 24-well plate at a density of 2×10^4 cells per well and cultured for 4 h. The samples were dehydrated with different concentrations of ethanol (30%, 50%, 70%, 80%, 90%, 95% and 100% v/v) and coated with gold.

2.3.3.2 CLSM The initial cell adhesion morphologies and cell skeleton arrangements of the bMSCs seeded on the samples were examined by confocal laser scanning microscopy (CLSM; FV 1000, Leica). The bMSCs were seeded on the samples in a 24-well plate at density of 2×10^4 cells per well. After 2, 4, and 24 h, the samples were incubation with primary antibodies (Vinculin, Abcam). Then, goat-anti-mouse fluorescein isothiocyanate RITC-conjugated secondary antibody (ZSGB-BIO, China) was added to all samples. The cells were stained with rhodamine-phalloidin antibody (FITC; Invitrogen). Then, the nuclei were stained with DAPI for another 8 min.

2.3.4 Cell proliferation

The viabilities of the bMSCs on the different samples were evaluated with Counting Kit-8 (CCK-8, Dojindo Laboratories Inc.,Kumamoto, Japan) assays. The bMSCs were seeded on the samples in a 24-well plate at density of 2×10^4 cells per well and cultured for 1, 4, 7 and 14 days. The optical density (OD) was determined using a spectrophotometer (Bio-Tek) at a wavelength of 450 nm.

2.3.5 Alkaline phosphatase (ALP) assay

BMSCs were seeded on the samples on a 24-well plate at density of 2×10^4 cells per well and cultured for 7 and

14 days. The samples were stained with a BCIP/NBT alkaline phosphatase assay kit (Beyotime, China) according to the manufacturer's instructions. The quantitative alkaline phosphatase (ALP) assays of the cells on the different samples were assessed with p-nitrophenyl phosphate (Nanjing Jiancheng Bioengineering Institute, China).

2.3.6 Extracellular matrix (ECM) mineralization

The bMSCs were seeded on the samples in a 24-well plate at density of 2×10^4 cells per well and cultured for 21 days. The calcium deposits were stained and quantify with 0.1% Alizarin red solution according to the manufacturer's instructions.

2.3.7 Quantitative real-time PCR

The bMSCs were seeded on the samples in a 12-well plate at a density of 4.5×10^4 cells per well and cultured for 7 and 14 days. Osteogenic-associated genes (ALP, Runt-related transcription factor2 [Runx2], osteopontin [OPN], Collagen-I [Col-1]) were analyzed using real-time reverse-transcriptase polymerase chain reaction (real-time RT-PCR). GAPDH was used as the housekeeping gene for normalization.

2.3.8 Western blot

The bMSCs were seeded on the samples in a 12-well plate at a density of 4.5×10^4 cells per well and cultured for 7 and 14 days. The expression levels of the osteogenesis-related proteins [rabbit OPN antibody (1:1000, Abcam), rabbit Runx2 antibody (1:1000, CST) and mouse BMP-2 antibody (1:1000, Abcam)] were validated by western blot. β-actin was used as an internal control.

2.3.9 In vivo studies

2.3.9.1 Animal surgery   Thirty 12-week-old male Sprague-Dawley rats were used in this study, and all animal procedures were performed in accordance with the standards of the Ethics Committee of the Fourth Military Medical University. All rats were randomly divided into the following five groups: PEEK, 25SP, 100SP, 25NP and 100NP. A hole with a diameter of 2 mm and a length of 5 mm was prepared at the distal femur using a dental drill, and a sterile sample (2 mm in diameter and 5 mm in length) was implanted. All the animals were sacrificed at 4 and 8 weeks.

2.3.9.2 Micro-CT evaluation   At 4 and 8 weeks, after the operation, the rats were sacrificed. The newly formed bone was determined by micro-computed tomography (μ-CT; Siemens, Germany).

2.3.10 Histological evaluation

At 8 weeks, after the μ-CT scan, the specimens were cut into 150-mm-thick sections. The sectioned samples were stained with van Gieson's picrofuchsin. Optical microscopy was conducted to observe and visualize the mineralized bone tissue and the percentage of bone-implant contact.

2.3.11 Statistics

All the experiments were independently performed in triplicates. The data were expressed as averages ± standard deviations. The software we used was IBM SPSS Statistics 22.0. The results of the in vitro and in vivo experiments were statistically analyzed by the one-way analysis of variance. $P \leq 0.05$ was considered to be statistically significant.
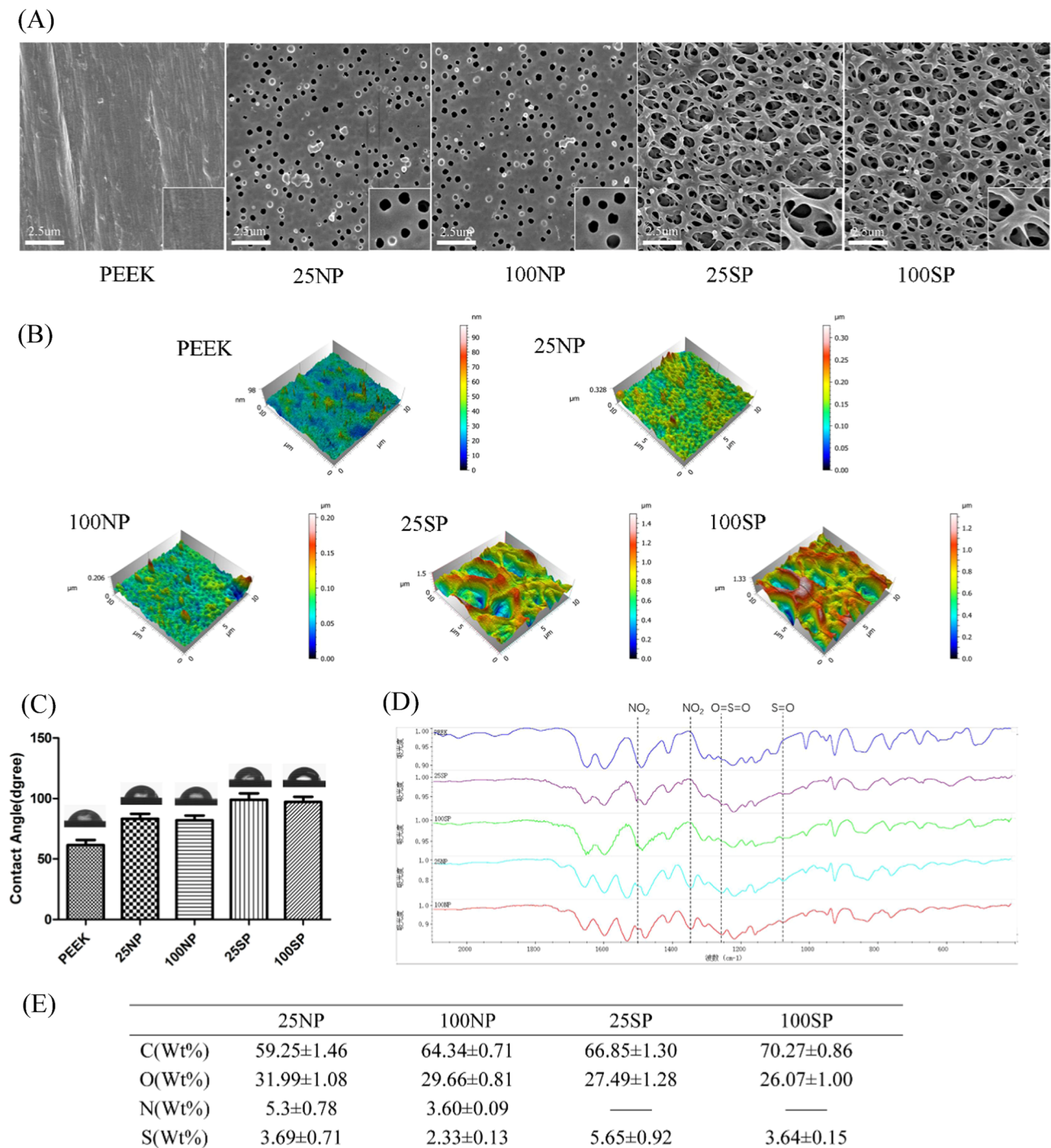
3 Results

3.1 Surface characterization

The surface morphologies of the SP, NP and PEEK samples under SEM are illustrated in Fig. 1. The surface of the untreated PEEK was smooth (Fig. 1a). Compared with the PEEK group, many porous structures were visualized in the NP and SP groups. The NP surface formed a monolayer nano-porous structure with a pore size of ~200–300 nm. The SP surface formed a 3D porous network structure with a pore size of ~0.5–2 μm. The morphologies of the samples were similar after high- or low-temperature hydrothermal treatment (25SP, 100SP; 25NP, 100NP).

Atomic force microscopy (AFM) images further demonstrated the surface morphologies and roughnesses (Fig. 1b). The PEEK group had a smooth surface. After the treatments, the surface morphologies of the NP and SP groups became rougher. The surface of the SP group exhibited greater roughness than the NP group possibly due to the larger and more complex pores.

The water contact angles are summarized in Fig. 1c. The water contact angle of the PEEK group increased after nitrification and sulfonation, respectively. The hydrothermal treatment had no effect on the water contact angle.

The FTIR spectrare presented in Fig. 1d. Among the five groups, except the PEEK group shared similar characteristic bands that included O=S=O dissymmetric stretching at 1255 cm^{-1} and S=O symmetric stretching at 1050 cm^{-1}. The nitro group was detected at 1500 cm^{-1} in the 25NP and 100NP groups. These data confirmed that the O=S=O, S=O and nitro groups were incorporated in

(A)

(B)

(C)

(D)

(E)

	25NP	100NP	25SP	100SP
C(Wt%)	59.25±1.46	64.34±0.71	66.85±1.30	70.27±0.86
O(Wt%)	31.99±1.08	29.66±0.81	27.49±1.28	26.07±1.00
N(Wt%)	5.3±0.78	3.60±0.09	——	——
S(Wt%)	3.69±0.71	2.33±0.13	5.65±0.92	3.64±0.15

Fig. 1 Surface characterization of the samples. **a** FE-SEM photographs acquired from the surface of PEEK, 25NP, 100NP, 25SP and 100SP. **b** Typical AFM image for the surface of PEEK, 25NP, 100NP, 25SP and 100SP. **c** Water contact angles of the different samples. **d** The comparative FT-IR spectra of the different samples. Blue:PEEK; violet:25SP; green:100SP; light blue:25NP; red:100NP. **e** Elemental compositions of the various samples detected by XRD

the polymer chain of the PEEK surface by sulfonation and nitrification.

The elemental compositions and distributions of the sample surfaces are presented in Fig. 1e. The 100NP group (high-temperature hydrothermal treatment) had lower contents of nitrogen and sulfur than the 25NP group. The nitrogen and sulfur concentration decreased from 5.3 ± 0.78 to 3.60 ± 0.09 and from 3.69 ± 0.71 to 2.33 ± 0.13, respectively. The sulfur content of the SP group decreased from 5.65 ± 0.92 to 3.64 ± 0.15 following high-temperature hydrothermal treatment.

3.2 Response of bMSCs in vitro

3.2.1 Cell adhesion

The initial adherence of the bMSCs to the samples is illustrated in Fig. 2a, b. The cells were incubated for 4 h and quantified with a DAPI assay. More bMSCs adhered to the surfaces of the 100NP and 100SP samples to the surface of the PEEK sample ($P < 0.05$). The 25NP (25SP) group exhibited fewer initially adhered cells than the 100NP (100SP) group.

3.2.2 Cell morphology

3.2.2.1 SEM   The morphologies of the cell change with the surface of the contact material. SEM images of the bMSCs on the samples are presented in Fig. 2c. The cells on the PEEK samples exhibited fewer filopodia, and some cells were spherical and unfolded. The cells on the NP and SP samples exhibited polygonal or spreading morphologies, abundant filopodia connected with each other, and ruffled osteoblast-like shapes. The cells in the 100NP group were also observed to adhere more closely than the cells in the100SP group.

3.2.2.2 CLSM   The initial adhesion morphologies of the bMSCs on the samples after 2, 4, and 24 h were monitored by confocal microscopy as illustrated in Fig. 2e. At 2 h, the cells on the 100NP and 100SP samples exhibited more microfilaments and stress fibers, and vinculin was clearly visualized. The cells on the 25NP and 25SP samples exhibited more actin filaments but fewer stress fibers. The cells in the PEEK group exhibited poorly developed cytoskeletons and vinculin. At 4 h, the cytoskeletons of each group were well developed. Binuclear cells were found in the 100NP and 100SP groups. The vinculin in the 100NP group was clearer and brighter than that in the 100SP group. At 24 h, many more bMSCs were observed on the NP and SP samples than on the PEEK samples, and their morphology were more similar with the morphology of osteoblasts. As illustrated in Fig. 2d, at 2, 4 h, the expression levels of vinculin were up-regulated in the 100NP group compared with the other groups.

3.2.3 Cell proliferation

Cell proliferation was measured with CCK-8 assays, and the results are presented in Fig. 2f. At 4, 7, and 14 days, the NP and SP groups exhibited significant differences from the PEEK group ($P < 0.05$). At 7 days, the 100SP samples exhibited more adhered cells than the 100NP samples ($P < 0.05$). At 14 days, there was no significant difference between the 100NP group and the 100SP group. At 1, 4, 7, and 14 days, the cell proliferation levels in the 100SP group were higher than those in the 25SP group. These findings indicate that high-temperature hydrothermal treatment increased the biocompatibilities of the materials.

3.2.4 ALP activity

As illustrated in Fig. 2g, the ALP activities of the NP and SP groups were greater than that of the PEEK group. The quantified ALP activity results are illustrated in Fig. 2i. The expression levels of ALP in the NP and SP groups were significantly increased compared with that in the PEEK group ($P < 0.05$). At 7 days, the expression level of ALP in the 100NP group was higher than that in the 100SP group. At 14 days, there was no significant difference between the 100NP and 100SP groups.

3.2.5 Extracellular matrix mineralization

As illustrated in the mineralization images (Fig. 2h), the NP and SP groups exhibited more mineralization of the nodules than the PEEK group. The quantitative analyses of Alizarin red staining are presented in Fig. 2g. The expression of ECM in the NP and SP groups was significantly different than that in the PEEK group ($P < 0.05$). The expression of ECM in the 100NP (100SP) group was higher than that in the 25NP (25SP) group ($P < 0.05$). There was no difference between the 100NP group and the 100SP group.

3.2.6 Osteogenesis-related gene expression levels

As shown in Fig. 3a, osteogenic-related genes, including ALP, Runx2, OPN, and COL-1, were quantified by real-time PCR and normalized to GAPDH. In general, the expressions of the osteogenic-related genes were affected by the different morphologies of the material surfaces. The expression levels of Runx2, ALP, OPN, COL-1 in the NP and SP groups were significantly ($P < 0.05$) increased compared with the expression levels in the PEEK control group at 7 days and 14 days. At 7 days, Runx2 and ALP were up-regulated in the 100NP group compared with the other groups ($P < 0.05$). At 14 days, OPN and COL-1 were up-regulated in the 100NP group compared with the other groups.

3.2.7 Western blot

The results were shown in Fig. 3b. At 7 days, the expression levels of OPN, Runx-2, and BMP-2 were up-regulated in the 100NP group compared with the other groups. At 14 days, OPN and BMP-2 were up-regulated in the 100NP groups compared with the other groups, while there were no obvious differences in Runx-2 among groups.

(A)

(B)

(C)

(D)

(E)

(F)
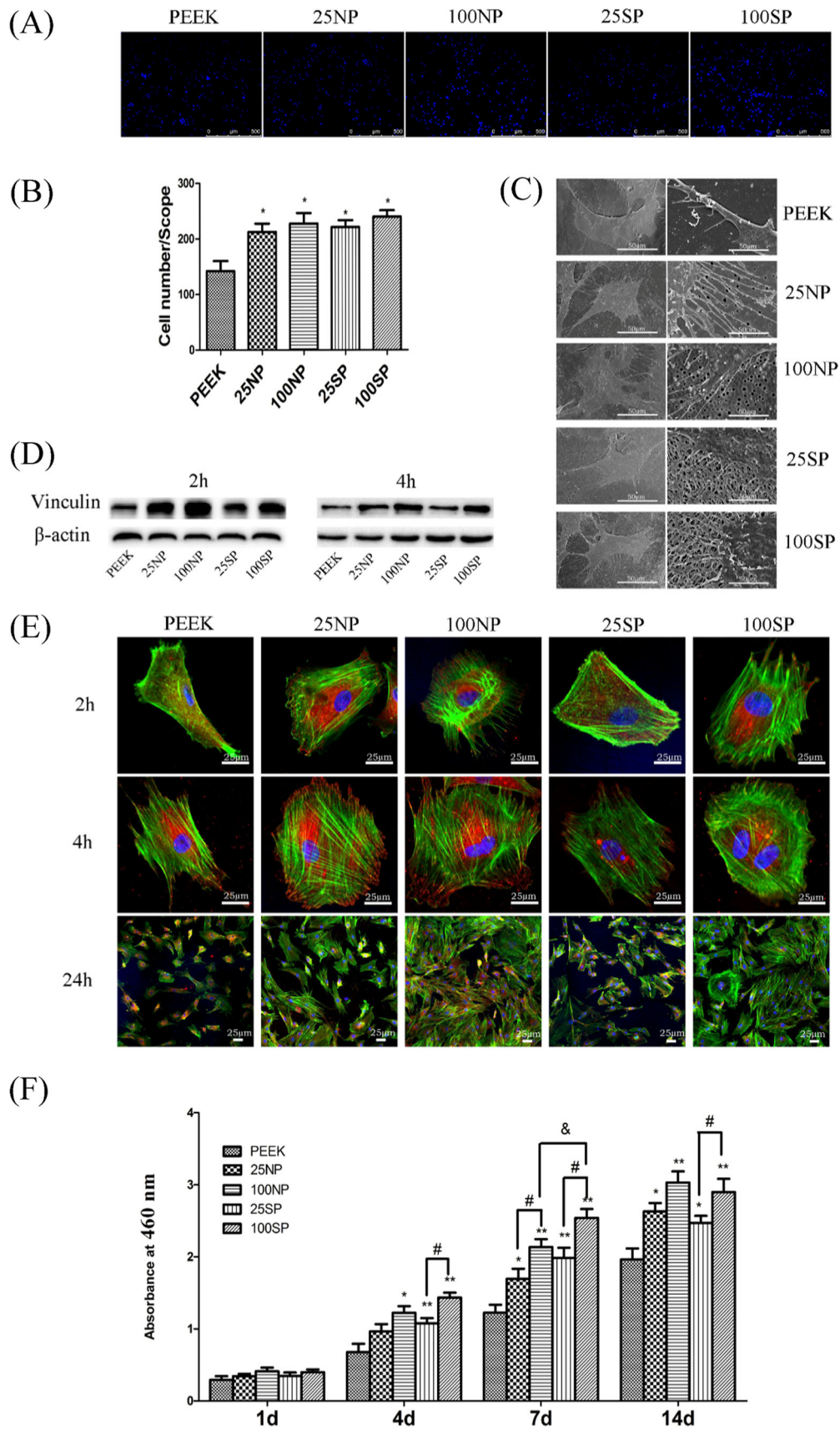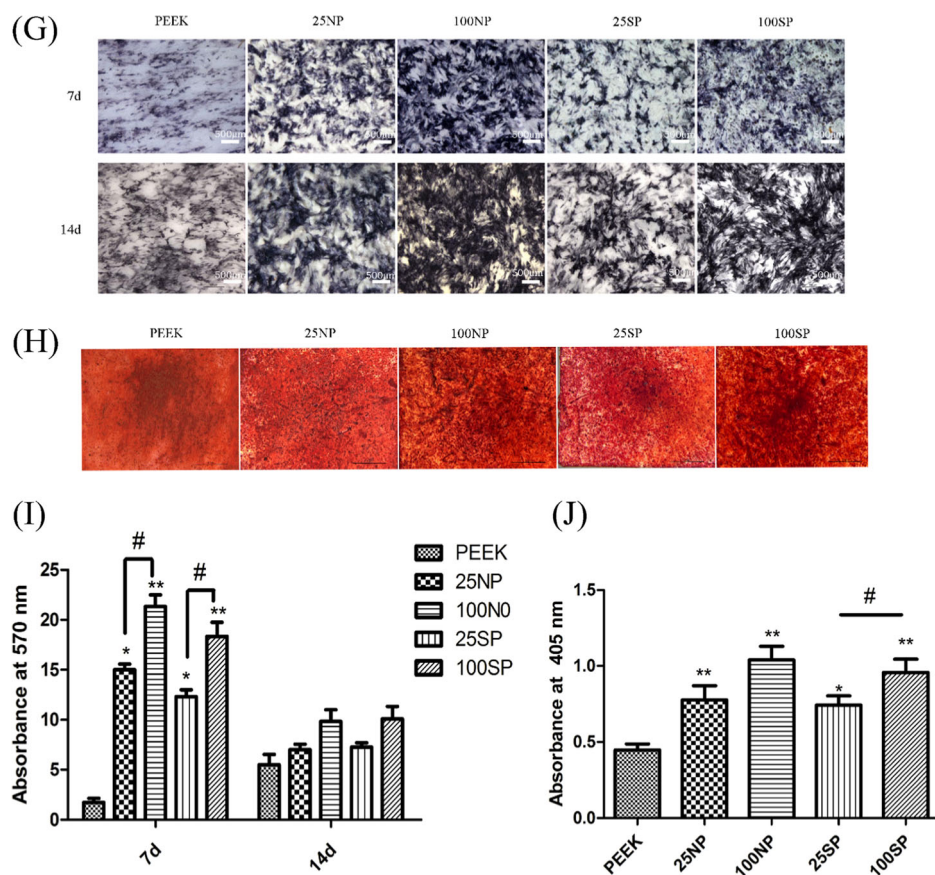
Fig. 2 Detection of biological behavior of cells on different material surfaces. **a** BMSC attachment after 4 h of incubation. The cells were stained with DAPI. **b** The initial numbers of adherent cells measured by counting the cells stained with DAPI after 4 h of incubation. *$P < 0.05$ vs PEEK. **c** SEM images of BMSC adhesion on the surfaces after 4 h, images taken at low magnification show the cellular morphology and high magnification show details of the cellular morphology. **d** Western blot analysis of the expression of the vinculin on different material surfaces. **e** CLSM images of BMSC adhesion on surfaces after 2 h, 4 h, and 24 h. The cells were stained for actin filaments (green), cell nuclei (blue) and vinculin (red). **f** BMSC proliferation after incubation for 1, 4, 7 and 14 days. *$P < 0.05$ vs PEEK; **$P < 0.01$ vs PEEK; #$P < 0.05$, 25NP vs 100NP, 25SP vs 100 SP; &$P < 0.05$ 100 NP vs 100SP. **g** Optical images of ALP-stained BMSCs after 7 and 14 days of incubation. **h** ECM mineralization: Optical images (**a–e**) of ARS-stained BMSCs after 21 days of incubation. **i** ALP activities of the different groups after culture for 7 and 14 days. *$P < 0.05$ vs PEEK; **$P < 0.01$ vs PEEK; #$P < 0.05$ 25NP vs 100NP and 25 SP vs 100SP. **g** Quantification of cell mineralization in the different groups after culture for 21 days. *$P < 0.05$ vs PEEK; #$P < 0.05$ 25 NP vs 100NP and 25SP vs 100SP

3.3 Micro-CT

The implantations in the femur are illustrated in Fig. 4a. The Micro-CT result are illustrated in Fig. 4b. The bone volumes/tissue volumes (BT/TV) were maintained in the 100NP and 100SP groups compared with the PEEK group ($P < 0.05$) at 4 and 8 weeks after surgery. The changes in bone volume around the implants in the 100NP group at 4 weeks dramatically higher than those in the PEEK group ($P < 0.05$). The trabecular separations (Tb.Sp) in the NP and SP groups at 4 and 8 weeks after implantation were significantly lower than those in the PEEK group ($P < 0.05$), and the Tb.Sp in the 100NP group at 4 weeks was also significantly lower than that of the 100SP group ($P < 0.05$). The increases in bone volumes in the 100NP, 100SP, 25NP, and 25SP groups were ~17.61%, 15.71%, 9.88%, and 7.14%, respectively, relative to the bone volume in the PEEK group at 4 weeks after implantation. The increases in bone volumes in the 100NP and 100SP groups were ~44% and 50%, respectively, relative to that in the PEEK group at 8 weeks after implantation.

3.4 Histology

Histological stainings of samples with Stevenel's blue and van Gieson's picrofuchsin are illustrated in in Fig. 4c. At 8 weeks, some of the PEEK directly contacted with the bone. However, there was a clear gap between the bone and the implant. All treated samples displayed direct bone-implant binding. Thicker new bone surrounded the 100NP implant.
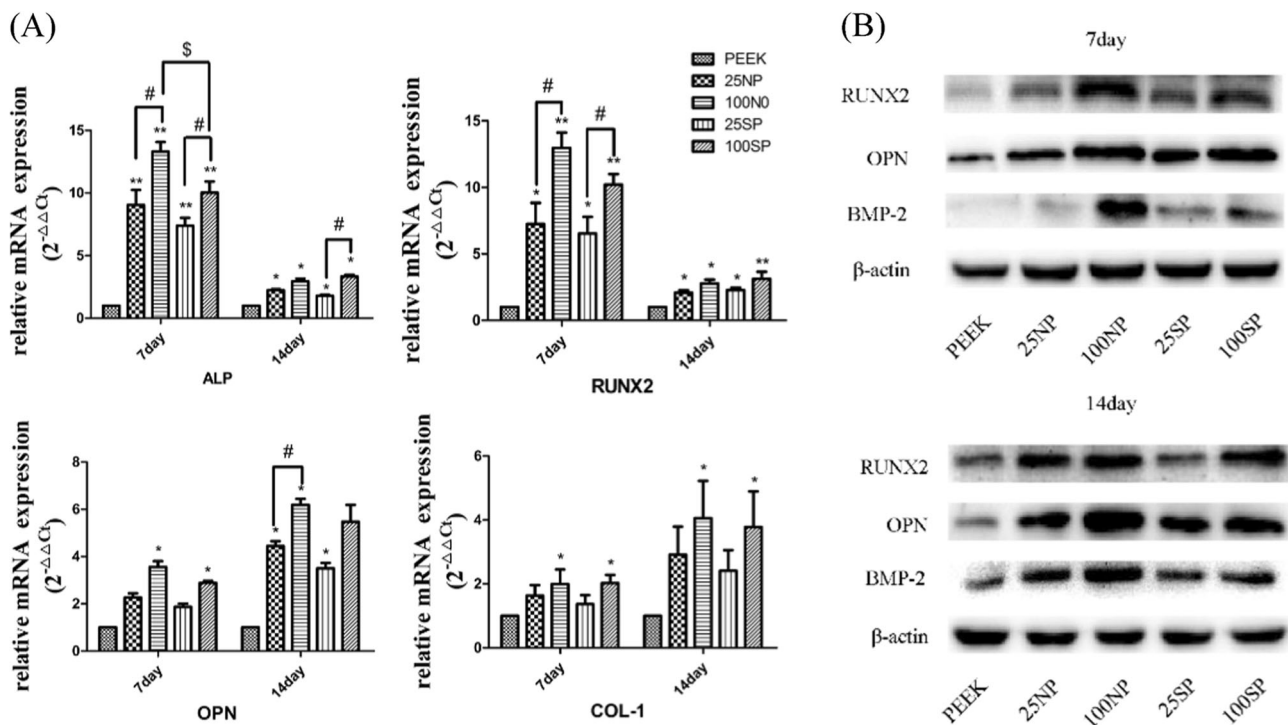
Fig. 3 Examination of bone related genes and proteins on the surface of different materials. **a** Real-time PCR detection of osteogenesis-related gene expressions in the BMSCs cultured on the samples for 7 and 14 days. $*P < 0.05$ vs PEEK; $**P < 0.01$ vs PEEK; $^{#}P < 0.05$ 25NP vs 100NP and 25SP vs 100SP; $^{##}P < 0.01$ 25NP vs 100NP and 25SP vs 100SP; $^{&&}P < 0.01$ 100NP vs 100SP. **b** Western blot analysis of the related protein secretions of the various groups after 7 and 14 days of incubation

4 Discussion

The physicochemical characteristics of the implant material and the surface microenvironment determine the biological behavior of the cells [11]. Numerous research efforts have recently been directed towards improving the bone/implant interface [12]. In this work, we exploited the advantage of the etching action of concentrated sulfuric acid on PEEK during sulfonation [13]. Subsequently, the main polymer chains of the SP samples were further substituted by nitration [14]. Three different surface morphologies were obtained by different treatments: a smooth surface, a monolayer nano-porous surface, and a 3D porous network surface. This study provided a new microenvironment for the cells. Initial cell adhesion is related to hydrophilicity and roughness of materials. According to our study, the hydrophilicity decreased and the roughness increased in SP group. In 100SP group, the number of initial cell adhesion was the highest. So, in present study, we speculate that roughness plays a leading role in cell adhesion.

Our results demonstrated that the high-temperature hydrothermal treatment surface (100S or 100N) corresponded to better bioactivity than that of the low-temperature hydrothermal treatment surface (25S or 25N) both in vivo and in vitro. These results are consistent with previous studies that pH variations with the concentration of

sulfur. High-temperature hydrothermal can reduce the content of sulfur in materials. As a result, the NP or SP samples that underwent high-temperature hydrothemal treatment exhibited good biocompatibility.

In vitro, the initial adhesion and proliferation of 100SP cells were better than that of 100NP and PEEK samples. The hydrophilicity of the treated materials was reduced. However, the porous structure increased the specific surface areas and roughnesses of the NP and SP surfaces. Porous surface provides more adsorption sites for cells and proteins. It further promotes adhesion and proliferation.

We found that the cell proliferation of SP in 7 days group was better than that in other groups. On the 7 day, the expression of ALP, Runx2 and BMP-2 increased significantly in 100NP samples. On the 14 day, the expression of OPN and BMP-2 in 100NP was significantly higher than that in other groups. We believe that nitrification can promote early differentiation of BMSCs. Due to the sulfonic groups (SO_3H) and nitro groups (NO_2) were incorporated into the polymer chain of the PEEK surface through sulfonation and nitrification. The benzene ring is directly connected with the SO_3H groups and the NO_2 groups, and these groups have inductive and conjugated effects [15]. The pi-electron cloud on the benzene ring is transferred to the groups. The main chain of the aromatics has a positive charge, and the branched chain groups have negative

(A)

(B)

(C)

PEEK   25NP   100NP   25SP   100SP
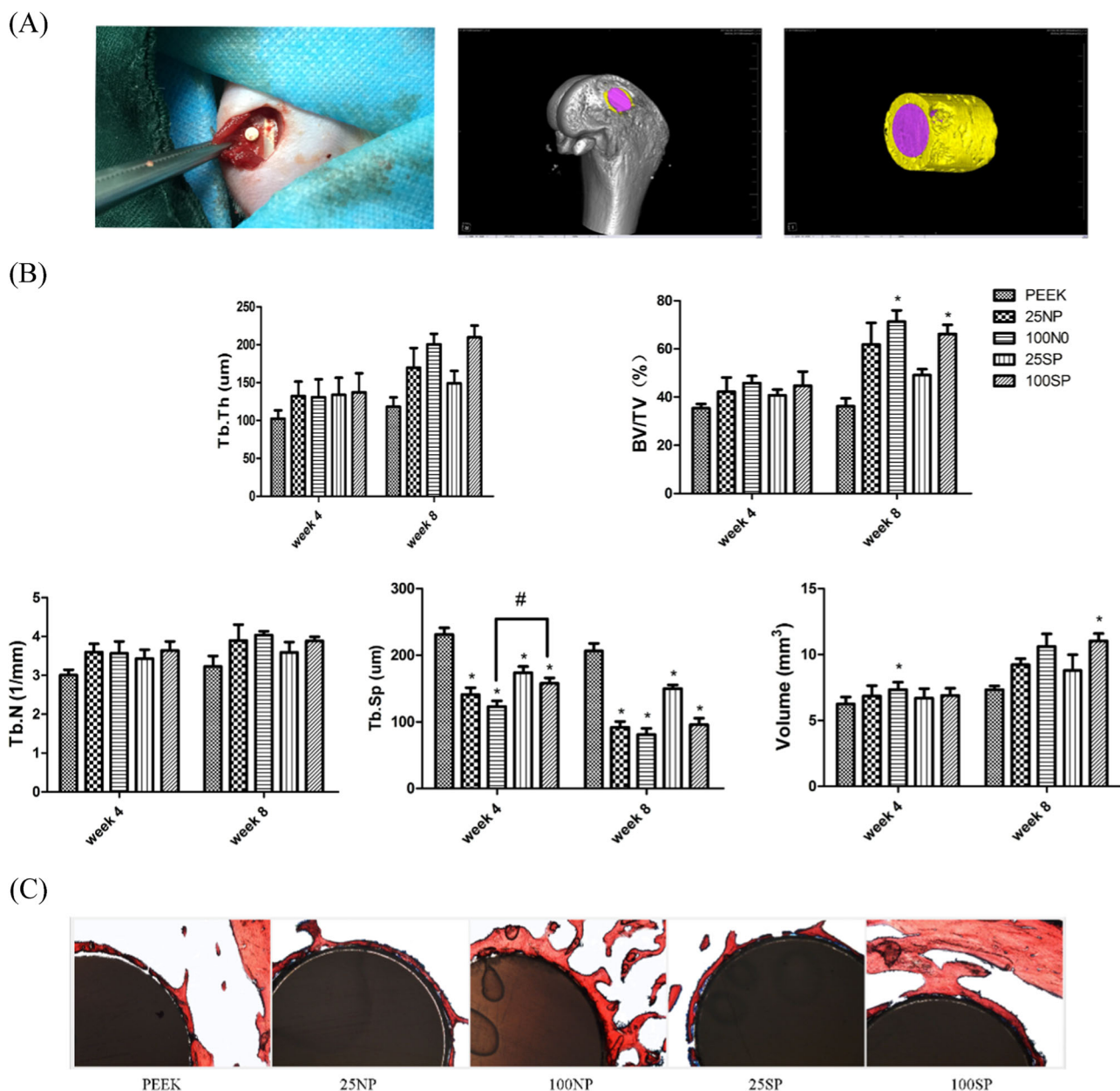
Fig. 4 Characterization of implants and the surrounding bones by Micro-CT and hard tissue sections. **a** Implantation of rat femur with PEEK implant. Micro-CT 2D and 3D reconstruction model showing the status of the implant (violet incolor) and bone (yellow in color). **b** Micro-CT results 4 and 8 weeks after implantation. *$P < 0.05$ vs PEEK; #$P < 0.05$ 100NP vs 100SP. **c** Hard tissue section of van Gieson's picrofuchsin stained around the implant after implantation for 8 weeks with the red color representing the newly formed bone

charges. The process of osseointegration involves a complex sequence of events [16]. The first event is the adsorption of proteins, calcium and phosphorus ions from the blood to the surface of the implant when the implant enters the body. Hence, protein with charged, calcium ions, and phosphorus ions are easily distributed on the NP surface. Such surfaces can accelerate the formation of fibrin clots by promoting the attachment of blood platelets and the subsequent release of their inner contents [17]. The early differentiation of 100SP is weaker than that of 100NP due

to the different surface morphology of materials. The irregular nano-topography, given its inherent biochemical information, could provide the signal to osteoblasts that the surface requires new bone formation [18]. Mechanical signals induced by surface topography are intracellularly converted into biochemical signals through a process called mechanotransduction [19]. The adhesion of cells to surfaces plays an important role in mechanotransduction mechanisms, as cell–ECM and cell–cell adhesion sites mediated by integrins and adherins, respectively, function as sites at

which forces and displacements are applied to the cell. We discovery that the expression of cell vinculin on 100NP increased. The microscopic results indicated that 100NP (200–300 nm) and 100SP (0.5–2 μm) samples exhibited more microfilaments and binuclear cells. Cells attached less tightly to the 100SP samples than to the 100NP samples. Cell morphology usually affects cell function and eventual tissue integration [20]. The cytoskeleton is receptive to the environment; signals are transmitted to the nucleus through the cytoskeleton, and the cytoskeleton can alter gene expression and cell fate [21]. Furthermore, Teo BK et al. revealed that nanogratings with a 250 nm line width on polydimethylsiloxane induced human mesenchymal stem cell (hMSC) differentiation through cell mechanotransduction that is modulated by the integrin-activated focal adhesion kinase (FAK) [22]. We speculate that the nanoporous (200–300 nm) microenvironment mediated differentiation is based on cellular mechanotransduction and early adhesion of proteins and ions. Subsequently, the differentiation process is regulated by integration. The integrin-mediated activation of focal adhesion kinase (FAK) promotes a high level of Runx2 expression. Runx2 further up-regulated the expression of ALP and OPN. Previous studies have proved that proliferation was inversely proportional to differentiation [21], which is a coincidence to our findings. BMSC differentiation is precisely regulated and orchestrated by mechanical and molecular signals in the extracellular environment [23]. Previous study has shown that irregular nanostructures can promote the differentiation of BMSCs. This study also shows that surface charges of materials also promote the proliferation of hepatocytes. At present, however, the specific mechanism is still unclear and needs further study [24].

The results of the in vivo rat femur model are consistent with the in vitro results. The difference in new bone volume was relatively small between the 100NP and 25NP groups at 8 weeks after implantation. The difference in new bone volume was more obvious between the 100SP and 25SP groups at 8 weeks after implantation. It is possible that the nitrocompounds on the 25NP surface had a short-term influence on the surrounding microenvironment, as diffusion and absorption were faster. The new bone of the Tb.Sp was gradually decreased and differed significantly between the PEEK, SP and NP groups. The TB/TV (Percent trabecular area), Tb.Th (Trabecular thickness) and Tb.N (Trabecular number) results further revealed that the new bone was denser around the NP samples. The surface of the PEEK was smooth and not conducive to new bone formation. In the 3D porous network structure on the SP surface, the pore diameter was large, and the new bone was widely distributed in a manner similar to that of cancellous bone. The nanoporous monolayer NP surface promoted cell differentiation

and mineralization, and the new bone was dense and similar to compact bone. Histological analyses revealed that there was no inflammation or necrosis observed in any of the implants. The implants exhibited no obvious toxic effects on the surrounding tissue. The results of the histological analyses are consistent with those of the micro-CT analysis. The percentages of bone-implant contact on the 100NP and 100SP implants were higher than that on the PEEK implants.

Chemical treatments are simple and cost-effective. It can form a modified surface layer uniformly on complex surfaces [25]. Acid treatments, such as HCl, H_2SO_4, HNO_3, HF and their mixes solutions, have been applied to Ti dental implants to obtain good bone bonding [26]. Furthermore, Kawai et al. recently showed that the bone-bonding capacity, osteoconduction and osteoinduction of the HCl/H_2SO_4-treated Ti were further increased when the metal was subsequently heat treated at 600 °C [27]. The obstacle to the clinical application of PEEK materials is poor biological activity, but its elastic modulus is better than that of Ti. It has been found that PEEK treated with sulfuric acid can form a 3D network structure and improve the biological activity of PEEK. In this study, PEEK was treated with sulfuric acid and nitric acid in turn, which formed layered nano-pore surface, enhanced early osteogenic activity of PEEK, and further enhanced the biological activity of the materials. Therefore, PEEK is a potential and excellent dental implants material.

5 Conclusions

After sulfonation, nitrification and subsequent water immersion, a nano-porous monolayer structure was obtained on the surface of PEEK. With further high-temperature hydrothermal treatment, the 100NP samples exhibited a remarkably improved cell/bone-PEEK interface in vitro and in vivo due to the effects of the nano-porous structure and the SO_3H and NO_2 functional groups. The surface treatment process described here is simple and inexpensive and may pave the way for further modifications of PEEK that will enable its use as dental implant material.

Compliance with ethical standards

Conflict of interest The authors declare that they have no conflict of interest

Ethical statement In this research all animal procedures were performed in accordance with the standards of the Ethics Committee of Shandong university (NO. GD201701, 02-27-2017).

Publisher's note Springer Nature remains neutral with regard to jurisdictional claims in published maps and institutional affiliations.

References

1. Wang H, Xu M, Zhang W, Kwok DT, Jiang J, Wu Z et al. Mechanical and biological characteristics of diamond-like carbon coated poly aryl-ether-ether-ketone. Biomaterials. 2010;31:8181–7.
2. Hieda A, Uemura N, Hashimoto Y, Toda I, Baba S. In vivo bioactivity of porous polyetheretherketone with a foamed surface. Dent Mater J. 2017;36:222.
3. Kurtz SM, Devine JN. PEEK biomaterials in trauma, orthopedic, and spinal implants. Biomaterials. 2007;28:4845–69.
4. Wang L, He S, Wu X, Liang S, Mu Z, Wei J et al. Polyetheretherketone/nano-fluorohydroxyapatite composite with antimicrobial activity and osseointegration properties. Biomaterials. 2014;35:6758–75.
5. Pezzotti G, Oba N, Zhu W, Marin E, Rondinella A, Boschetto F et al. Human osteoblasts grow transitional Si/N apatite in quickly osteointegrated Si3N4 cervical insert. Acta Biomaterialia. 2017;64:411–29.
6. Gui N, Xu W, Abraham AN, Myers DE, Mayes E, Xia K et al. A comparative study of the effect of submicron porous and smooth ultrafine-grained Ti-20Mo surfaces on osteoblast responses. 2018;106:2020–33.
7. Alves AC, Thibeaux R, Toptan F, Pinto AMP, Ponthiaux P, David B. Influence of macroporosity on NIH/3T3 adhesion, proliferation, and osteogenic differentiation of MC3T3-E1 over biofunctionalized highly porous titanium implant material. J Biomed Mater Res Part B Appl Biomater. 2018;107:73–85.
8. Zhao Y, Wong HM, Wang W, Li P, Xu Z, Chong EYW et al. Cytocompatibility, osseointegration, and bioactivity of three-dimensional porous and nanostructured network on polyetheretherketone. Biomaterials. 2013;34:9264–77.
9. Torstrick FB, Evans NT, Stevens HY, Gall K, Guldberg RE. Do surface porosity and pore size influence mechanical properties and cellular response to PEEK? Clin Orthop Relat Res®. 2016;474:1–11.
10. Evans NT, Torstrick FB, Lee CSD, Dupont KM, Safranski DL, Chang WA et al. High strength, surface porous polyether-ether-ketone for load-bearing orthopaedic implants. Acta Biomater. 2015;13:159–67.
11. Lai M, Cai Y, Hermann CD, Cheng A, Walker M, Olivares-Navarrete R et al. Cell morphology correlates with integrin expression on microrough titanium surfaces. In: Iadr/aadr/cadr General Session and Exhibition. 2013.
12. Schwarting T, Lechler P, Struewer J, Ambrock M, Frangen TM, Ruchholtz S et al. Bone morphogenetic protein 7 (BMP-7) Influences tendon-bone integration in vitro. PLoS One. 2015;10: e0116833.
13. Ouyang L, Zhao Y, Jin G, Lu T, Li J, Qiao Y et al. Influence of sulfur content on bone formation and antibacterial ability of sulfonated PEEK. Biomaterials. 2016;83:115.
14. Tsai JC, Kuo JF, Chen CY. Nafion®/nitrated sulfonated poly(ether ether ketone) membranes for direct methanol fuel cells. J Power Sour. 2009;194:226–33.
15. Krygowski TM, Oziminski WP. Substituent effects in 1-nitro-4-substituted bicyclo[2.2.2]octane derivatives: inductive or field effects? J Mol Model. 2014;20:2352.
16. Rosa AL, Kato RB, Castro Raucci LM, Teixeira LN, de Oliveira FS, Bellesini LS et al. Nanotopography drives stem cell fate toward osteoblast differentiation through $\alpha1\beta1$ integrin signaling pathway. J Cell Biochem. 2014;115:540–8.
17. Zhu Y, Zhang K, Zhao R, Ye X, Chen X, Xiao Z et al. Bone regeneration with micro/nano hybrid-structured biphasic calcium phosphate bioceramics at segmental bone defect and the induced immunoregulation of MSCs. Biomaterials. 2017; 147:133.
18. Gittens RA, Olivaresnavarrete R, Schwartz Z, Boyan BD. Implant osseointegration and the role of microroughness and nanostructures: lessons for spine implants. Acta Biomater. 2014;10:3363–71.
19. Liu Q, Wang W, Zhang L, Zhao L, Song W, Duan X et al. Involvement of N-cadherin/β-catenin interaction in the micro/nanotopography induced indirect mechanotransduction. Biomaterials. 2014;35:6206–18.
20. Zhao L, Liu L, Wu Z, Zhang Y, Chu PK. Effects of micropitted/nanotubular titania topographies on bone mesenchymal stem cell osteogenic differentiation. Biomaterials. 2012;33:2629.
21. Malec K, Góralska J, Hubalewskamazgaj M, Głowacz P, Jarosz M, Brzewski P et al. Effects of nanoporous anodic titanium oxide on human adipose derived stem cells. Int J Nanomed. 2016;11: 5349–60.
22. Teo BK, Wong ST, Lim CK, Kung TY, Yap CH, Ramagopal Y et al. Nanotopography modulates mechanotransduction of stem cells and induces differentiation through focal adhesion kinase. Acs Nano. 2013;7:4785–98.
23. Zhang W, Dong R, Diao S, Du J, Fan Z, Wang F. Differential long noncoding RNA/mRNA expression profiling and functional network analysis during osteogenic differentiation of human bone marrow mesenchymal stem cells. Stem Cell Res Ther. 2017;8:30.
24. Ffb H, Papenburg B, Vasilevich A, Hulsman M, Zhao Y, Levers M et al. Mining for osteogenic surface topographies: in silico design to in vivo osseo-integration. Biomaterials. 2017;137:49.
25. Spriano S, Yamaguchi S, Baino F, Ferraris S. A critical review of multifunctional titanium surfaces: New frontiers for improving osseointegration and host response, avoiding bacteria contamination. Acta Biomater. 2018;79:1–22.
26. Refai AK, Textor M, Brunette DM, Waterfield JD. Effect of titanium surface topography on macrophage activation and secretion of proinflammatory cytokines and chemokines. J Biomed Mater Res Part A. 2004;70:194–205.
27. Kawai T, Takemoto M, Fujibayashi S, Neo M, Kokubo T. Bone-bonding properties of Ti metal subjected to acid and heat treatments. J Mater Sci Mater Med. 2012;23:2981–92.